



TriDurLE

**National Center for Transportation
Infrastructure Durability & Life-Extension**

Project ID: 2020-MST-06

**AUTOMATED DETECTION AND CHARACTERIZATION OF CRACKS ON
CONCRETE USING LASER SCANNING**

Final Report

By

Xiong Zhang, Ph.D., P.E.
Professor of Civil Engineering
Missouri University of Science and Technology

for

National University Transportation Center TriDurLE
Department of Civil & Environmental Engineering
405 Spokane Street PO Box 642910
Washington State University Pullman, WA 99164-2910

October 25, 2022

PUBLICATION REPORT OPTION

The work in this research was summarized as a technical paper, which has been accepted for publication in *ASCE's Journal of Infrastructure Systems*, formatted in the style used by the National Center for Transportation Infrastructure Durability & Life-Extension (TriDurLE).

Acknowledgements

This work was supported by the National Key R&D Program of China (No. 2017YFC1501303). The Dr. Yunfeng Ge is grateful to the Chinese Scholarship Council for providing an opportunity to conduct the research described in this report as a visiting research scholar at the Missouri University of Science and Technology in Rolla, Missouri. Mr. Ruiyang Zhang is acknowledged for his help in data collection.

Disclaimer

The contents of this report reflect the views of the authors, who are responsible for the facts and the accuracy of the information presented. This document is disseminated under the sponsorship of the Department of Transportation, University Transportation Centers Program, in the interest of information exchange. The U.S. Government assumes no liability for the contents or use thereof.

Table of Contents

PUBLICATION REPORT OPTION.....	2
Acknowledgements	3
Disclaimer	4
Table of Contents	5
List of Figures	6
List of Tables.....	7
Executive Summary.....	8
Chapter. 1 Introduction.....	9
1.1 Problem Statement.....	9
1.2 Objectives and Scope	11
1.3 Expected Contributions	11
1.4 Report Overview	11
Chapter. 2 Literature Review	13
Chapter. 3 Methodology and Procedures	16
3.1 Point Clouds Collection.....	17
3.2 Point Normal Calculation	19
3.3 Cracks and Dents Extraction Based on Point Normal Variance.....	21
3.4 Small-Scale Dents Removal	24
3.5 Cracks Characterization.....	26
3.5.1 Projected Dimension of Crack.....	26
3.5.2 Real Dimension of Crack	27
3.5.3 Manual Crack Measurement.....	30
Chapter. 4 Case Study	31
Chapter. 5 Summary and Conclusions	40
References	42

List of Figures

Figure 1 Flow chart of the proposed method in this study.	17
Figure 2 Point cloud collection of cracks on a concrete ground.....	18
Figure 3 Point cloud mapped based on different parameters	20
Figure 4 Cracks and dents extraction from the point cloud.....	24
Figure 5 Dents removal from the point cloud of boundaries.....	26
Figure 6 Crack characterization using projection and curve-skeleton methods	29
Figure 7 Point clouds collection of cracks in the stair case.....	32
Figure 8 Variance of point normal vectors and computational time of point normal calculations with different neighboring points	33
Figure 9 Cracks detection from point clouds in the stair case.....	35
Figure 10 Projection of the crack point clouds.....	36
Figure 11 Curve-skeleton of the crack point clouds.....	37
Figure 12 Ten cross-sections selected in the point clouds of cracks	38

List of Tables

Table 1 Summary of scan parameters and point clouds for two cases.	19
Table 2 Summary of dimensions of cracks.	27
Table 3 Computational time of crack detection and characterization for two cases.	39

Executive Summary

Accurate cracks detection and characterization on concrete is essential for the maintenance, safety, and serviceability of various infrastructures. In this research, an innovative approach was developed to automatically measure the cracks from 3D point clouds collected by a laser scanner. The approach integrates several techniques to characterize the cracks, which include the deviation on point normal determined using k-nearest neighbor (kNN) and principal components analysis (PCA) algorithms to identify the cracks, and principal axes and curve-skeletons of cracks to determine the projected and real dimensions of cracks, respectively. The coordinate transformation was then performed to estimate the projected dimensions of cracks. Curve-skeletons and cross-sections of cracks were extracted to represent the real dimensions. Two cases of surface cracks were used to validate the developed approach, and analysis results have indicated that there are good agreements with real situations.

Chapter. 1 Introduction

1.1 Problem Statement

Detection and characterization of crack dimension and pattern in aging infrastructure such as pavement, bridges and tunnels, play an important role in evaluating durability safety, durability, and service life. At present, crack detection can be classified into two major categories: contact and non-contact surveying.

In terms of contact methods, several instruments have been developed for contact inspection to measure the crack geometry, such as crack magnifier (Valença et al. 2013), width ruler (Nakaniwa et al. 2014), feeler gauge (Bandis et al. 1983), and electronic sensor (Ritdumrongkul 2007). Although these contact inspection methods can provide high precision measurement results with low cost, this technique suffers several limitations: (1) they are laborious and time consuming; (2) sometimes they impose high safety risk to operators, especially under the conditions of inaccessible regions and inclement weather; (3) most methods have limited measurement range and sensitivity; and, (4) the results are highly subjective, more depending on the engineers' skill and experience.

With the advances of electro-optical technology in the past few decades, diverse non-contact methods are available to determine the location and geometries of cracks, including two-dimensional (2D) image processing technique and analysis of reconstructed three-dimensional (3D) data. There have been increasing interests in the non-contact methods due to their ability to effectively address the aforementioned problems (Nishiyama et al. 2015). Moreover, non-contact methods have made it possible to automate the crack detection through the introduction of some numerical algorithms.

2D image analysis is very popular for the crack detection due to its versatility and extremely low cost. A widely used assumption for pavement crack detection on 2D images is that the crack has a lower intensity than the local background. Such an assumption provides the basis for many algorithms, including the thresholding methods (Oliveira and Correia 2009), segmentation-based approaches (Kirschke and Velinsky 1992), filter-based algorithms (Zalama et al. 2014), minimal-path methods

(Avila et al. 2014), texture-anisotropy approach (Nguyen et al. 2009), and the CrackTree (Zou et al. 2012). Another assumption for detecting cracks on 2D images is that the crack represents a sharp change in intensity. Following this assumption, several crack detection methods were developed with the use of edge detectors (Santhi et al. 2012) or wavelet transforms (Zhou et al. 2006).

Nevertheless, all infrastructures as well as cracks on them are three dimensional. Image taking can only result in 2D images, and the depth is lost. As a result, 2D image analyses cannot provide accurate 3D measurement for advanced analyses. In addition, the 2D image analysis methods only consider the color data and completely ignored the geometric information, which lead to a gap when applying them to existing structures (Valença et al. 2017). Furthermore, the 2D image analysis methods highly depend on the image quality and lighting conditions. Images are taken in the dark environment (in the tunnel, cloudy day, and shadow) will cause the weakness in intensity difference between cracks and background. As a result, the image processing technique still faces many challenges in reality practices (Mohan et al. 2018).

Another category of algorithms detects cracks using 3D pavement surface data. Compared with 2D images, 3D surface data are less vulnerable to lighting conditions and present more useful information as well as fewer noises in terms of crack detection (Zhang and Wang 2017a). The consistency and repeatability of 3D pavement surface data provide a better opportunity to successfully detect cracks. The depth-checking methods (Jahanshahi et al. 2013), interactive crack detection algorithm (Zhang et al. 2016a), hybrid crack detection procedures (Sollazzo et al. 2016), and 3D shadow modeling (Zhang et al. 2017) were all proposed in recent years for detecting cracks on 3D surfaces.

In terms of 3D surface data acquisition, laser scanning has been extensively used to reconstruct the 3D model of cracks. Laser scanning method points a small laser at a surface and measure the time it takes the laser to return to its source. The principle is simple. However, it requires special equipment which is very cost-prohibitive. In addition, the color and intensity information is completely ignored.

Properly characterizing cracks to find the 3D dimensions of cracks is critical as well. Cracks are often curves rather than straight lines, and their 3D geometry changes irregularly. It is therefore unreasonable to measure the crack using the projection dimensions. Due to the complexity and diversity of crack patterns, crack characterization is a challenging task even for human operators. At present, majority of studies focused on the crack detection, while the characterization of cracks after they are

detected was rarely investigated. 2D image analyses discussed previously cannot provide accurate 3D models for cracks and therefore cannot be used for accurate crack characterization.

1.2 Objectives and Scope

The objective of this study was to develop an innovative approach to automatically map the cracks on concrete structures based on the 3D point clouds gathered using laser scanning, and accurately characterize cracks including their projected and real dimensions. To achieve the project goal, several tasks were completed. First, the literature was reviewed to collect information on crack detection and characterization methods such as contact and noncontact methods. Then, a surface crack was used as an example to navigate the procedures of image data collection, processing, analysis. A conventional crack survey was then conducted to validate the results obtained from this approach. The paper further presents a case study of detecting and characterizing more complicated cracks to demonstrate the feasibility of this approach.

1.3 Expected Contributions

The expected research results will be a innovative photogrammetry method to automatically detect and characterize cracks in aging infrastructure such as pavement and bridge surface. The method only requires use of low-cost commercially available digital camera to generate high accuracy 3D point clouds for crack detection. Post-processing algorithms will be developed to automatically calculate the real lengths as well as the real width and depth of a crack at any arbitrary locations. The method will provide transportation authorities the information they need to maintain the transportation infrastructure more effectively and economically, and better understanding of the performance of infrastructure to inform future designs and materials.

1.4 Report Overview

This report includes five chapters and a list of references. Chapter 1 presents an introduction of the study and the scope of the work. Chapter 2 provided a thorough literature review on crack detection and characterization methods such as contact and noncontact methods. In Chapter 3, a surface crack was used as an example to navigate the procedures of image data collection, processing, analysis. A conventional crack survey was then conducted to validate the results obtained from this approach. Chapter 4 further presents a case study of detecting and characterizing more complicated cracks to

demonstrate the feasibility of this approach. Finally, the summary and conclusions of the study are presented in Chapter 5.

Chapter. 2 Literature Review

Cracking by far makes up the majority of failure issues in many infrastructures such as pavements, bridges, structures, and tunnels because of its tendency to spread and the wide variety of elements that can cause cracking. Accurately detecting, continually monitoring, and timely assessing cracking before the “critical condition” is reached, extends the service life of infrastructure and reduces life-cycle costs, gives transportation authorities the information they need to maintain it more effectively and economically, allows engineers to intervene before a catastrophic failure, and provides a better understanding of the performance of assets to inform future designs and materials.

To date, the detection of crack dimensions and patterns can be classified into two major categories: contact and non-contact methods. In the contact methods, traditionally transportation infrastructures are visually inspected and manually maintained under traffic control with the aid of heavy lifting equipment or costly inspection equipment. Some contact inspection methods, such as crack magnifier (Valença et al. 2013), width ruler (Nakaniwa et al. 2014), feeler gauge (Bandis et al. 1983), and electronic sensor (Ritdumrongkul 2007), can provide high precision measurement results with low costs. However, these techniques suffer from challenges such as tediousness and subjectivity. With the advances of electro-optical technology in the past few decades, diverse non-contact methods are available to determine the location and geometries of cracks, including two-dimensional (2D) image processing techniques and analysis of reconstructed three-dimensional (3D) data (Nishiyama et al. 2015; Napolitano and Glisic 2019). 2D image analysis is very popular for crack detection due to its versatility and extremely low cost. Based on the assumptions that the crack has a lower intensity than the local background and the crack represents a sharp change in intensity, various numerical algorithms and detection methods have been developed. Some examples include intensity thresholding methods (Oliveira and Correia 2009), segmentation-based approaches (Kirschke and Velinsky 1992), filter-based algorithms (Zalama et al. 2014), minimal-path methods (Avila et al. 2014), texture-anisotropy approach (Nguyen et al. 2009), the CrackTree (Zou et al. 2012), artificial neural network (Kaseko and Ritchie 1993; Lee and Lee 2004; Dung 2019), support vector machine (Li et al. 2017; Hoang et al. 2018), and deep-learning (Zhang et al. 2016; Huang et al. 2018; Cha et al. 2017). However, all these image-based

methods only consider the color data overlooking the importance of geometric information, which leads to a gap when applying them to existing structures (Valença et al. 2017). Nevertheless, all infrastructures as well as cracks on them are three-dimensional (3D). 2D image analyses cannot provide accurate 3D measurements for advanced analyses (Valença et al. 2017; Mohan et al. 2018).

The limitations of 2D image processing techniques bring out the advent of 3D reconstruction, which are less vulnerable to lighting conditions and present more useful information as well as fewer noises in terms of crack detection (Wang 2004; Zhang et al. 2019). The depth-checking methods (Jahanshahi et al. 2013), interactive crack detection algorithm (Zhang et al. 2017a), hybrid crack detection procedures (Sollazzo et al. 2016), and 3D shadow modeling (Zhang et al. 2017b) were all proposed in recent years for detecting cracks on 3D surfaces. Among many of them, laser scanning, a remote sensing technique, is capable of making a long-distance measurement with high resolution. Recently, it has gained more attention in civil and geological engineering areas as a promising tool to reconstruct the 3D model of cracks through collecting the dense point clouds of concrete surfaces (Laefer et al. 2014; Gui et al. 2018; Ge et al. 2018). Olsen et al. (2010) mapped the cracks on concrete based on the intensity of point cloud which provided a sharp contrast between unruptured surfaces and cracks. Kim et al. (2014) employed both angle and distance deviations to locate the regular defects (square and round shapes) on concrete surfaces under experimental conditions. Jovančević et al. (2017) detected the dents and scratches from point clouds using a region growing algorithm in which the local normal and curvature parameters were used as the evaluation indexes. Artificial intelligence algorithms have also been introduced to analyze the point clouds for cracks recognition, such as the wavelet neural network (Laflamme et al. 2012), recurrent neural network (Zhang et al. 2019), deep-learning (Zhang et al. 2017a; Fei et al. 2019).

Although laser scanning has demonstrated its effectiveness in cracks detection in previous studies, some methods were performed under the laboratory environment, which had difficulties in identifying complete cracks over the whole region (Zou et al. 2012). In addition, 3D reconstruction always involves a huge amount of points, and some undesired noises are also introduced during data collection, resulting in the inefficiency and limitations of data processing (Rabah et al. 2013). More research efforts are needed to refine and improve for the purpose of practical application.

Properly characterizing cracks to find the 3D dimensions of cracks is critical as well. Cracks are

often curves rather than straight lines, and their 3D geometry changes irregularly. It is therefore inaccurate to measure the crack using the projected dimensions. At present, the majority of studies focused on crack detection. However, the characterization of cracks after they are detected has been rarely further investigated due to the complexity and diversity of crack patterns. In addition, 2D image analyses discussed previously cannot provide accurate 3D models for cracks and therefore cannot be used for accurate crack characterization.

Chapter. 3 Methodology and Procedures

In this study, a method was developed to automatically identify and measure the cracks on concrete structures from point clouds collected by laser scanning. Two main steps are involved in this method: crack detection and crack characterization (Figure 1). In the first step of crack detection, the point clouds of cracks and concrete structures are collected using a terrestrial laser scanner (TLS). The normal vector of each point is calculated using the k-nearest neighbor (kNN) and principal components analysis (PCA) algorithms. All objects with a significant change of point normal are then extracted from the point clouds based on the normal variance, including cracks, dents, and horizontal edges (intersections of different planes). The small-scale dents can be removed by setting a volume threshold. As for the horizontal edges which do not belong to cracks, they can be removed by specifying a specific location range since these edges have regular shapes and similar z-axis values. In the second step of crack characterization, a coordinate transformation algorithm is used to determine the rotation and translation matrixes, and the projected dimension of cracks is then measured to roughly estimate the area of cracks. In addition, L_1 -median skeleton algorithms are used to find the curve-skeleton of cracks to calculate the actual length of cracks, and 10 cross-sections are randomly selected to determine the actual width and depth. An example was next used to elaborate the procedures.

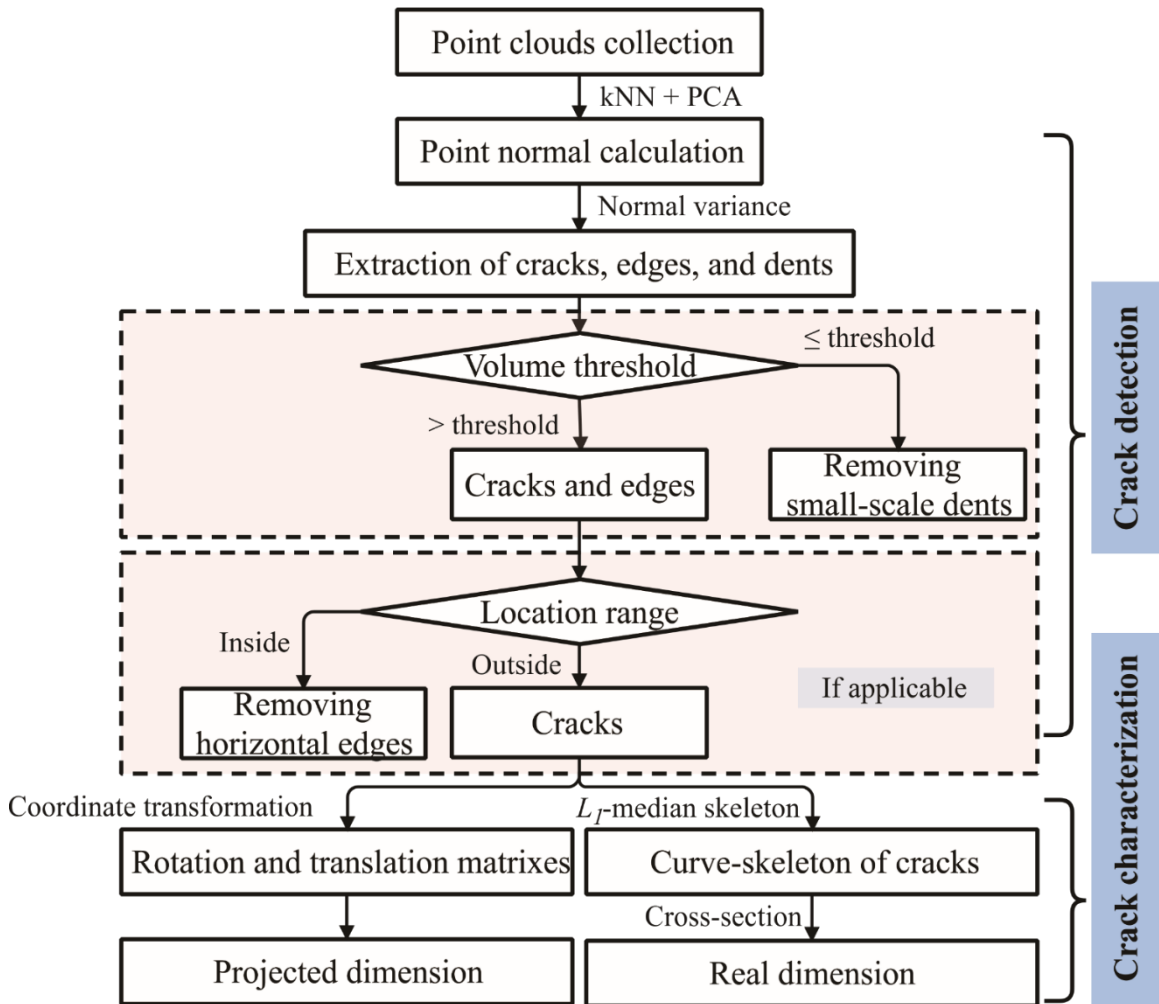


Figure 1 Flow chart of the proposed method in this study.

3.1 Point Clouds Collection

A surface crack located on a paved concrete ground in a building entrance area was selected to demonstrate the procedures of the developed approach. This crack was in a curved shape with an average length of 4.180 m and an average width of 0.009 m. Figure 2a shows the picture of the crack, and the area within a red rectangle is the scanning region. A phase-shift TLS (FARO Focus3D S120) was used to collect the point cloud of this crack. The maximum measuring range of this scanner is 120 m under the conditions of low ambient light and normal incidence. Its resolution — the interval between adjacent points, can reach 0.3 mm at a 10 m scanning distance. Scanning parameters and basic information of raw point cloud are listed in Table 1. Figure 2b shows the top view of the point cloud of the scanning region on the ground collected using this scanner. Total 527,320 effective points were

generated for this area after denoising, allowing to capture the details of geometry information of this crack (Figure 2c). Figure 2d shows the point cloud of the same scanning region from the side view. As can be seen in Figures 2c & 2d, the crack can be distinguished from point clouds based on the difference of geometric irregularity and discontinuity between the crack and the surrounding. It is noted that the laser can even reach the inside of cracks to collect point clouds, which is usually difficult for normal image-based techniques due to the low illumination.

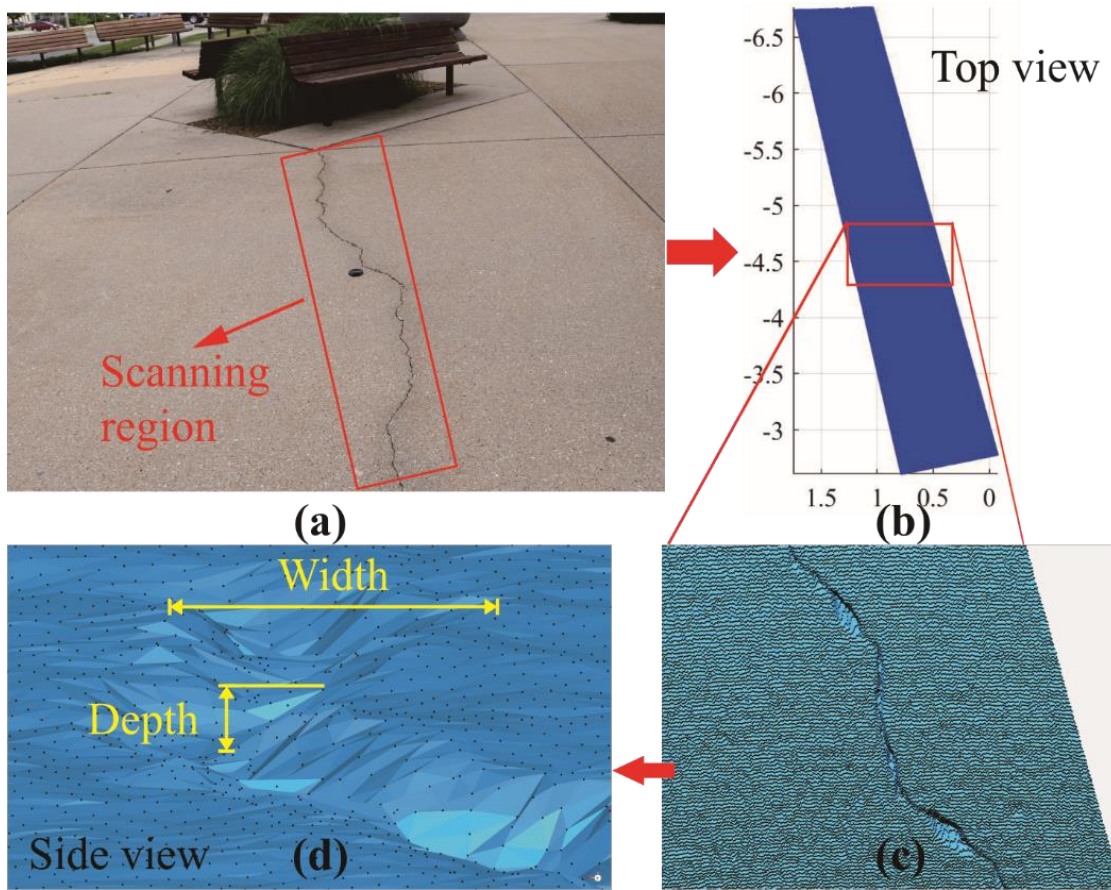


Figure 2 Point cloud collection of cracks on a concrete ground : (a) scanning region, (b) top view of point cloud in the scanning region, (c) details of point cloud in the crack region, and (d) side view of point cloud in the scanning region.

Table 1 Summary of scan parameters and point clouds for two cases.

Cases	Resolution setting	Quality	Speed (kpt/sec)	Scan time	Scan size (pt)	Resolution (mm/10m)	File size (MB)	Point amount
Ground surface	1/2	4×	122	5'46''	1702×4127	3.068	345	5858350
Stair	1/2	3×	244	2'11''	848×1994	3.068	89	1585865

3.2 Point Normal Calculation

Several parameters are available to describe the discontinuous geometry of cracks, including point normal, point curvature, point intensity, and depth. Figure 3 compares the sensitivity of these parameters to this example crack. As shown in Figure 3, the magnitude of point normal on the crack was larger than that on the surrounding surface, and the direction of point normal was different between the crack area and non-crack area, indicating the point normal has adequate robustness to capture the difference between the cracks and the surrounding. Nevertheless, the crack and non-crack areas were difficult to distinguish using other three parameters (i.e., point curvature, point intensity, and point depth). Thus, the point normal was selected for the purpose of crack detection in this study.

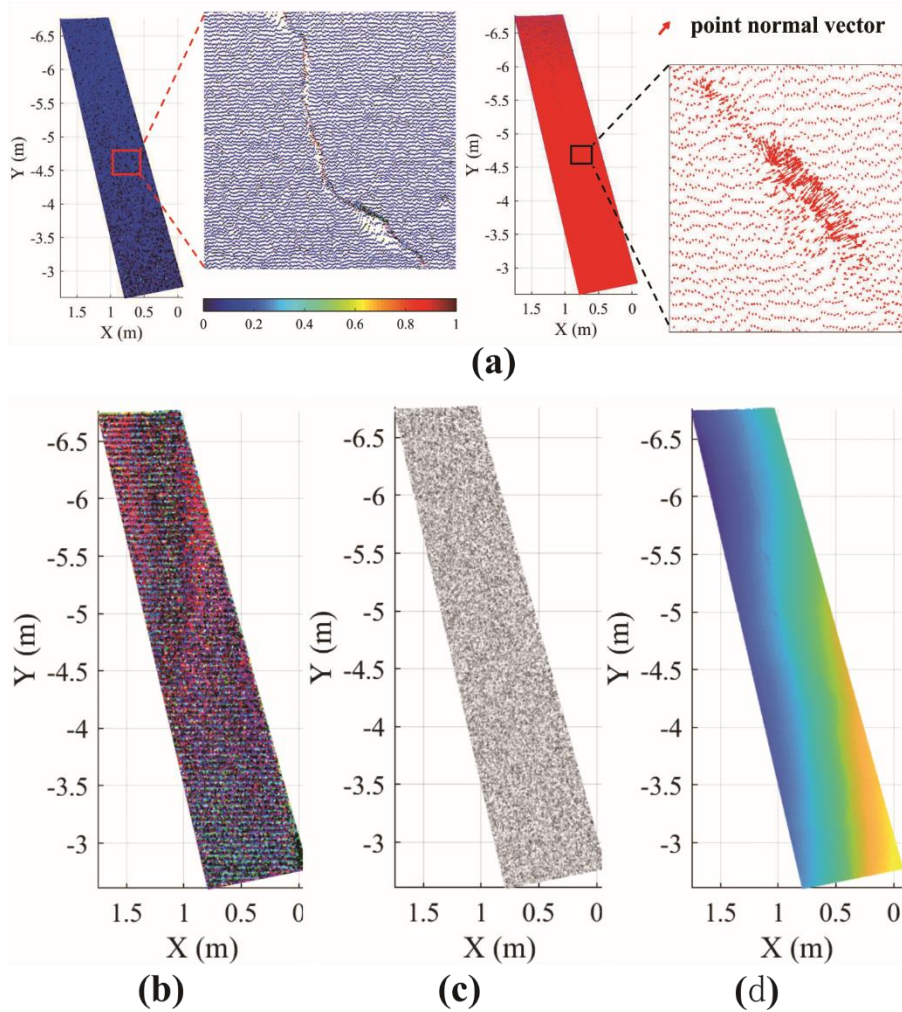


Figure 3 Point cloud mapped based on different parameters : (a) point normal, (b) point curvature, (c) point intensity, and (d) point depth.

The normal of a point is represented by the normal of the fitting plane to this point and its neighbors. For the grid data (organized point clouds), 4-connected or 8-connected points can be treated as neighbors. In addition, the surrounding points can be determined using the kNN algorithm by specifying the number of closest points or searching radius in the origin point clouds. In this study, to avoid the interpolation errors caused by data gridding, kNN algorithm was used to search the N , the number of nearest neighbor points of a query point. The kNN algorithm is a non-parameter classification approach and has been widely used in many applications (Deng et al., 2016), which is available in MATLAB software using the `knnsearch` function. The normal of the query point was then determined by calculating the normal of the fitting plane to the point set (query point and its neighbor points). Estimation of point normal was therefore reduced to an implementation of the PCA of the point set, and

the eigenvector corresponding to the smallest eigenvalue of the covariance matrix of the point set was the point normal (Klasing et al., 2009). PCA algorithm relates the process of determining the principal components of a given data and can be performed by the `pca` function in MATLAB software. Geometrically, the points on the concrete plane featured a similar normal direction which was approximately perpendicular to the plane, and the similar normal magnitude as shown in Figure 3a. Thus, the places with significant changes on normal (high normal deviation) can be regarded as the crack area. The direction and magnitude of the point normal in this area are different from those in the concrete plane due to the geometric irregularity and discontinuity.

3.3 Cracks and Dents Extraction Based on Point Normal Variance

Significant changes of point normal occur on the cracks and dents (small-scale damaged areas) due to the geometrical discontinuity, while the points on the concrete plane have similar normal values. Therefore, the point normal variance can be used as an indicator to describe the changes in these features. For a given point, the point normal variance ($Var(n_p)$) can be calculated by Eq. (1):

$$Var(n_p) = \frac{\sum_{i=1}^{N+1} (n_i - \bar{n})^2}{N+1} \quad (1)$$

where, \bar{n} is the average of normal of the given point and its nearest points, n_i is the point normal of the i th nearest point of a given point, and N is the number of the nearest points which can be determined through the kNN algorithm, as introduced in the previous section.

Because of the roughness of the ground surface, larger point normal variances were observed not only on the cracks, but also the dents on the concrete plane. The k-means clustering analysis was then performed to separate the whole point cloud into two groups — ground surfaces with lower normal variances and crack and dent regions with higher normal variances, based on the calculation of the point normal variance (Cheung 2003). The k-means algorithm is a popular tool to conduct the data partition based on the distance to the cluster center (Hamerly and Elkan, 2004), and the function of `kmeans` is available for this algorithm in MATLAB software. Both point normal and normal variance calculations highly depend on the N , and careful attempts are required to select the optimal one. For the surface crack, the point cloud was not spaced with a uniform interval since the scanning distance between the scanner and the object varies with locations, causing differences in the point density which was defined

as the number of points per unit volume associated with the query point in a 3D level (Eq.2).

$$D_p = \frac{N_p}{V_p} \quad (2)$$

where, D_p indicates the point density, and N_p is the point number within a 3D space with a volume of V_p . For the convenience of calculation, Eq.2 was simplified as:

$$D_p = \frac{1}{4/3 \cdot \pi \cdot r^3} \quad (3)$$

where, r is the radius of the sphere under consideration and can be estimated based on the 4th nearest neighbor distance of the query point. The average point density for the whole point cloud was calculated based on the average ($\text{mean}(\text{dist}_{4th})$) and standard deviation ($\text{std}(\text{dist}_{4th})$) of 4th nearest neighbor distances (dist_{4th}) of all points in the point cloud (Eq. 4) (Ester et al., 1996; Riquelme et al., 2014):

$$r = \text{mean}(\text{dist}_{4th}) + 2 \cdot \text{std}(\text{dist}_{4th}) \quad (4)$$

Figure 4a illustrates the point density distribution in the ground crack case. The point density gradually decreased from the bottom to the top which had a further scanning distance to the scanner, and the average point density of entire point clouds was 3.3969 points/cm³. Accordingly, scanning with a shorter distance acquired more points under the same condition, indicating more details on the ground surface were captured. To eliminate the effects of point density differences on the crack detection, it is suggested to calculate the point normal and point normal variance based on the point clouds with similar average point densities. In this case, the point cloud started from -6.7648 m and ended at -2.6071 m with a length of 4.1577 m along the Y-axis direction. Theoretically, the more segments the point cloud was equally divided into, the closer the average point density of each segment was, and however the more processing time was required accordingly. To maintain a balance between precision and efficiency, the point cloud with a significant difference in point density was suggested to be divided into at least three segments. Therefore, the point cloud of the concrete ground case was discretized into three equal segments along Y-axis with a similar average point density for each one: 0.2382 points/cm³ ($Y \leq -5.4$ m), 2.5188 points/cm³ ($-5.4 \text{ m} < Y < 4.0$ m), and 7.4336 points/cm³ ($Y \geq 4.0$ m). Figures 4b - 4d show the cracks and dents detection with the same number of neighbor points for the entire scanning region after

clustering analyses: $N = 5, 10,$ and $20,$ respectively. A high N value means more points are involved to calculate the point normal, ignoring the local difference between the query point and its neighbor points and vice versa. For the regions with a high point density ($Y \geq -4.0$ m), a smaller N increased the difference in the point normal, leading to too many small-scale dents identified in addition to cracks. On the other hand, the cracks in the regions with a low point density ($Y \leq -5.4$ m) could be mistakenly removed from the point cloud when N was specified as a larger value, emphasizing too much on the global features of point normal rather than local features. Therefore, the optimal N should be selected according to the point density. Serials of point clouds with different average point densities were generated from segment data of this example (region within $-5.4 \text{ m} < Y < 4.0 \text{ m}$ in this example) using the `pcdownsample` function in MATLAB software, and the original average point densities were 2.5188 and 46.4127 points/cm³, respectively. The corresponding minimum and maximum N were estimated for each point cloud through multiple adjustments until good crack detections were achieved. Linear relationships were observed between the average point density (D_{ap}) and N , as expressed in Eq. 5 Figure 4e):

$$\begin{cases} N_{\max} = 11.45 \cdot D_{ap} + 2.06 \\ N_{\min} = 2.03 \cdot D_{ap} + 4.92 \end{cases} \quad (5)$$

According to Eq. 5, the appropriate range of N for each segment was determined based on the average point density of the point cloud. Accordingly, the range of neighbor points numbers for each segment was set as $5 \leq N \leq 5$ ($Y \leq -5.4$ m), $10 \leq N \leq 31$ ($-5.4 \text{ m} < Y < 4.0 \text{ m}$), and $20 \leq N \leq 87$ ($Y \geq -4.0$ m). Because the computational time increased with the increase of N , the minimum of N was selected to enhance the data processing efficiency. In this manner, reasonable results of point normal variance calculation and cracks and dents detection were achieved via the k-means clustering analysis (Figures 4f and 4g).

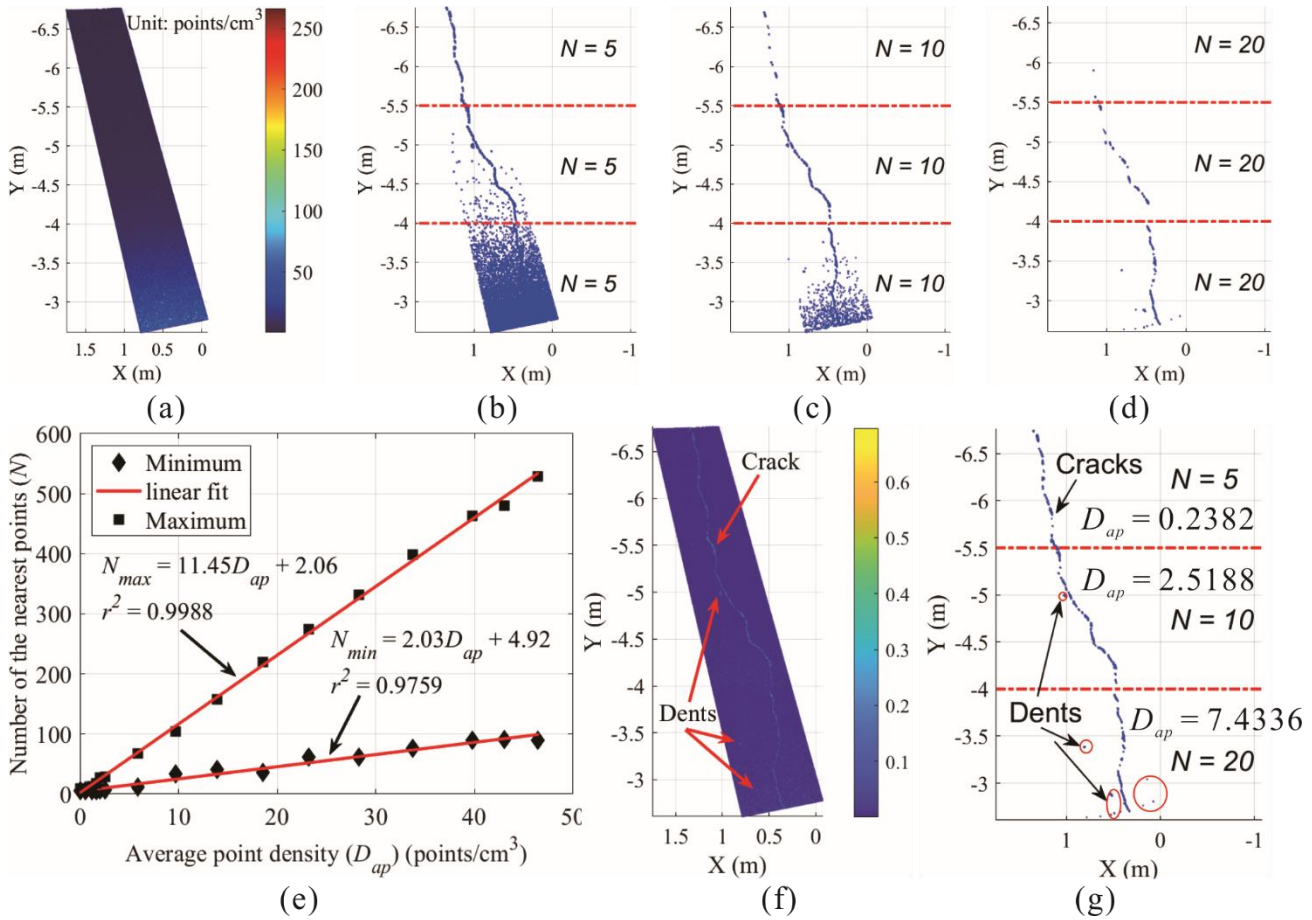


Figure 4 Cracks and dents extraction from the point cloud : (a) point density distribution, (b) clustering analysis with $N = 5$, (c) clustering analysis with $N = 10$, (d) clustering analysis with $N = 20$, (e) relationship between average point density and number of the nearest points; (f) normal variance calculation with different N , and (g) cracks and dents detection after clustering analysis.

3.4 Small-Scale Dents Removal

The geometric characteristics varied from cracks to dents: dents were small-size and isolated pits on the ground surface, and the cracks were characterized by continuous curves. In addition, dents were distributed on the ground surface one by one with less connectivity, resulting in a smaller volume. Therefore, cracks can be separated from dents based on the differences in their dimensions, such as aspect ratio, area, and volume. In this study, the volume was selected as the judging parameter to remove the points on the small-scale dents. To calculate the volume, 3D models of cracks and dents were reconstructed using the alpha-shape algorithm. The alpha-shape algorithm is an effective tool to define both convex and non-convex envelope of points depending on the alpha value. An alpha value of

1 generates a convex hull (Edelsbrunner et al. 1983). However, due to the concave shape of cracks and dents, a non-zero alpha radius was automatically determined to estimate their concave hulls and compute their volumes using the criticalAlpha function in MATLAB software. Then, an automated method was proposed to determine the volume threshold for removing the dent points via calculating the maximum value of volume. When the convex hull volume of points was lower than the volume threshold, these points were considered as the dents and were removed from the point clouds.

In this example, the majority of dents were located on the bottom region of the crack. Figure 5 demonstrates the procedure of dents removal using the detected boundaries in the range from -2.64 to -3.13 along the Y-axis. Figure 5a shows the originally detected point clouds of crack and dents in this region. The polyhedrons with different sizes in Figure 5b were the concave hulls of the crack and dents reconstructed using the alpha-shape algorithm with a 0.004 m alpha radius. It can be seen that more continuous and larger polyhedra were generated for crack points, compared to the dent points. Figure 5c illustrates the volume distributions of the dent and crack polyhedra. Because of the specific geometric characteristics, the volumes of dent polyhedra were much smaller than the volumes of the cracks. Therefore, the polyhedron with the largest volume was treated as the crack, which was automatically determined by calculating the maximum volume. Meanwhile, the dents — the polyhedrons with smaller volumes — were removed from the point cloud of boundaries (Figure 5d). Figure 5e shows the point cloud of the entire crack after all dents were removed in this example. A good agreement was observed between the crack detection in Figure 5d and the real situation in Figure 2a, revealing the alpha-shape algorithm can accurately capture the geometrical features of crack and dents and distinguish them.

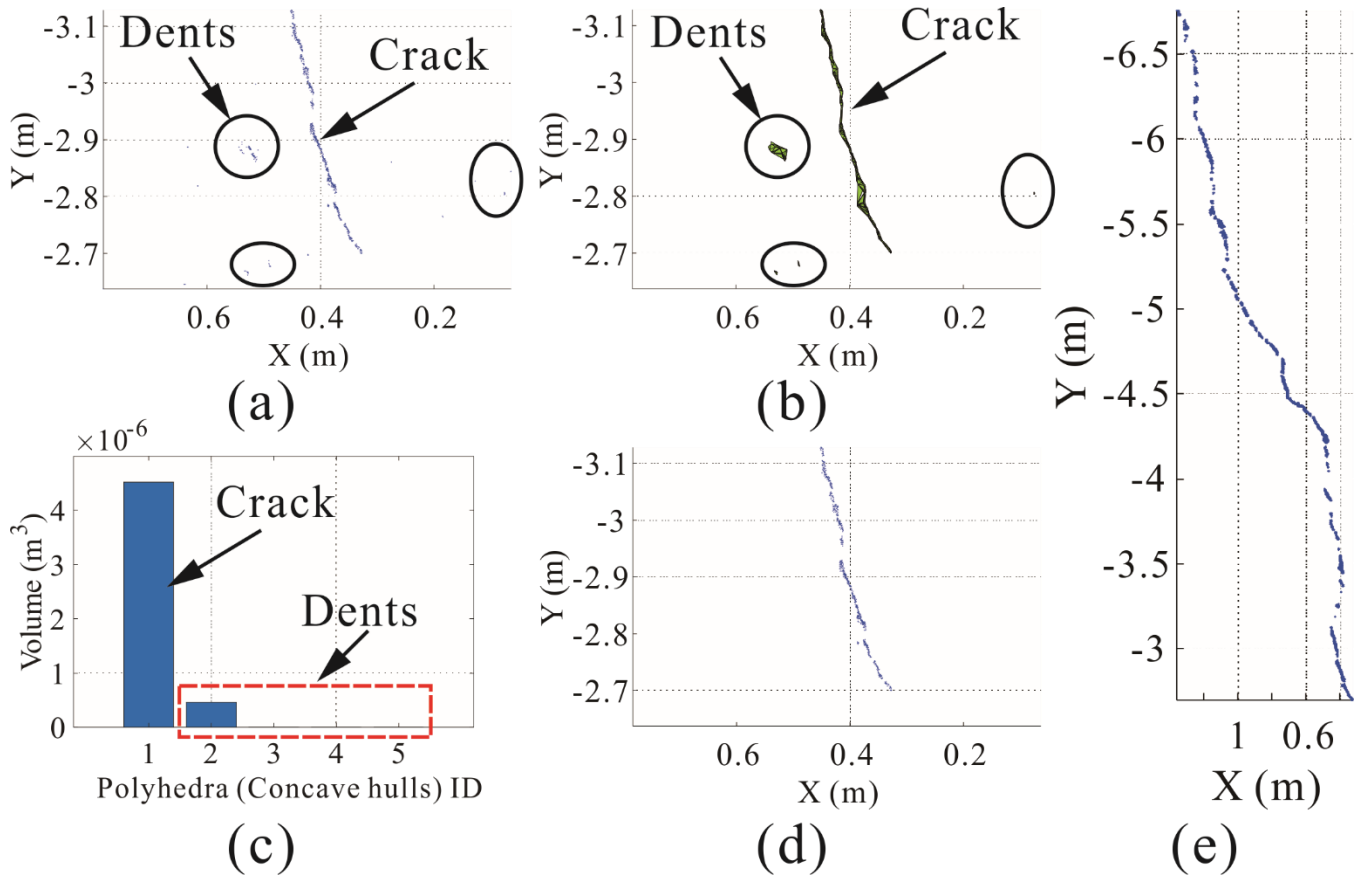


Figure 5 Dents removal from the point cloud of boundaries : (a) point clouds of crack and dents, (b) 3D reconstruction of crack and dents, (c) volume distribution of dents and crack, (d) point cloud of the portion of the crack, and (e) point cloud of the whole crack.

3.5 Cracks Characterization

Both the projected and real dimensions of the crack were determined in this study. Results were compared with those from manual measurement during the crack condition survey.

3.5.1 Projected Dimension of Crack

The point cloud of the detected crack was projected into a horizontal plane to measure its projected dimensions. To perform the projection, a new coordinate system is needed to be defined, in which the major axis (longitudinal direction) of a crack is selected as the X-axis, the middle axis is the y-axis, and the minor axis is the z-axis. In Euclidean space, point cloud projection is treated as a rigid transformation that can be implemented based on the rotation matrix \mathbf{R} and translation matrix \mathbf{T} (Eq. 6).

$$PC^* = PC \cdot \mathbf{R} + \mathbf{T} \quad (6)$$

Where, PC^* is the point clouds of cracks after projection, PC is the original point clouds of cracks, \mathbf{R} is represented by an orthogonal matrix which can be determined using the PCA algorithm, and \mathbf{T} is estimated by the difference of minimum on XYZ between original and rotated point clouds. The largest distances of projected point cloud along the major, middle, and minor axis are regarded as the projected length, width, and depth of the crack, respectively.

Figure 6a illustrates the results of coordinate projection of the crack on the concrete ground. The black lines indicate the principal axes of the crack and the line length is its projected dimension. As summarized in Table 2, the projected dimension of this crack was 4.185 m in length, 0.338 m in width, and 0.013 m in depth. The projected dimension represents the minimum external cuboid containing the cracks on the concrete structures.

Table 2 Summary of dimensions of cracks.

Cases	Location	Point amount	Manual measurement			Projection algorithm			Curve-skeleton algorithm		
			Length (m)	Width (m)	Depth (m)	Length (m)	Width (m)	Depth (m)	Length (m)	Width (m)	Depth (m)
Ground surface	-	4183	4.18	0.009	-	4.185	0.338	0.013	4.285	0.008	0.003
	Upper	3917	0.275	0.015	0.013	0.268	0.07	0.05	0.339	0.018	0.012
Stair	Middle	4096	0.273	0.012	0.012	0.272	0.039	0.03	0.298	0.011	0.017
	Lower	18778	0.369	0.014	0.025	0.357	0.085	0.038	0.440	0.021	0.012

3.5.2 Real Dimension of Crack

Due to the fact that the crack is often a curve rather than a straight line, the curve-skeleton of the point cloud was adopted to calculate the real length of cracks. Curve-skeleton is a simplified version of a 3D object with 0 volume, which provides a compact and intuitive representation of complex geometries and can capture their essential geometric features (Cornea et al., 2007; Au et al., 2008). Extraction of

curve-skeleton is useful for reducing the data dimension in many applications, such as path planning, shape registration and retrieval, and plant morphological traits (Falcão et al., 2017). In this study, the L_1 -median skeleton algorithm was used to extract the curve-skeletons of cracks (Huang et al., 2013), and the open-source code of this algorithm is available on the website (<https://vcc.tech/research/2013/L1skeleton>). L_1 -median, also known as the geometric median, is the point with a minimum sum of the distance to all surrounding points. L_1 -median can be approximately calculated using an iterative procedure (Bose et al., 2003). Figure 6b demonstrates the curve-skeletons (green lines) extraction of cracks from the point cloud, and the accumulation distance among the key points (red dots) was determined to represent the actual length of cracks. The actual length of this crack is 4.285 m as shown in Table 2.

The cracks on concrete structures are often characterized by irregular shapes, causing great data dispersion only via a single measurement. The dimension of the crack varied from location to location, and it was very difficult to obtain the accurate dimensions of the crack only through one single cross-section. Therefore, multiple measurements were required to perform to enhance the measuring accuracy. Through trial and error, it was found that the crack width tended to be stable when more than 10 cross-sections were chosen (Figure 6c). Therefore, in this study, 10 cross-sections were randomly selected to eliminate the measurement error due to the data dispersion. Figure 6d shows that locations of 10 cross-sections were randomly chosen along the crack to determine its real width and depth, each of which was perpendicular to the crack. These sections can be defined by the points with distance to the plane on either side less than the tolerance, which was set as 1 mm in this study. Two cross-sections were selected to demonstrate the typical geometry features in the Y-Z plane and were roughly v-shaped as shown in Figure 6c. The maximum distances along the width (Y-axis) and depth (Z-axis) direction at each section were determined, and the average of 10 sections was considered as the real width and depth of the crack. The green circles are the randomly selected cross-sections, and the points located on the circles can be extracted based on the distance tolerance (red points). The crack has an actual width of 0.008 m and an actual depth of 0.003 m as summarized in Table 2.

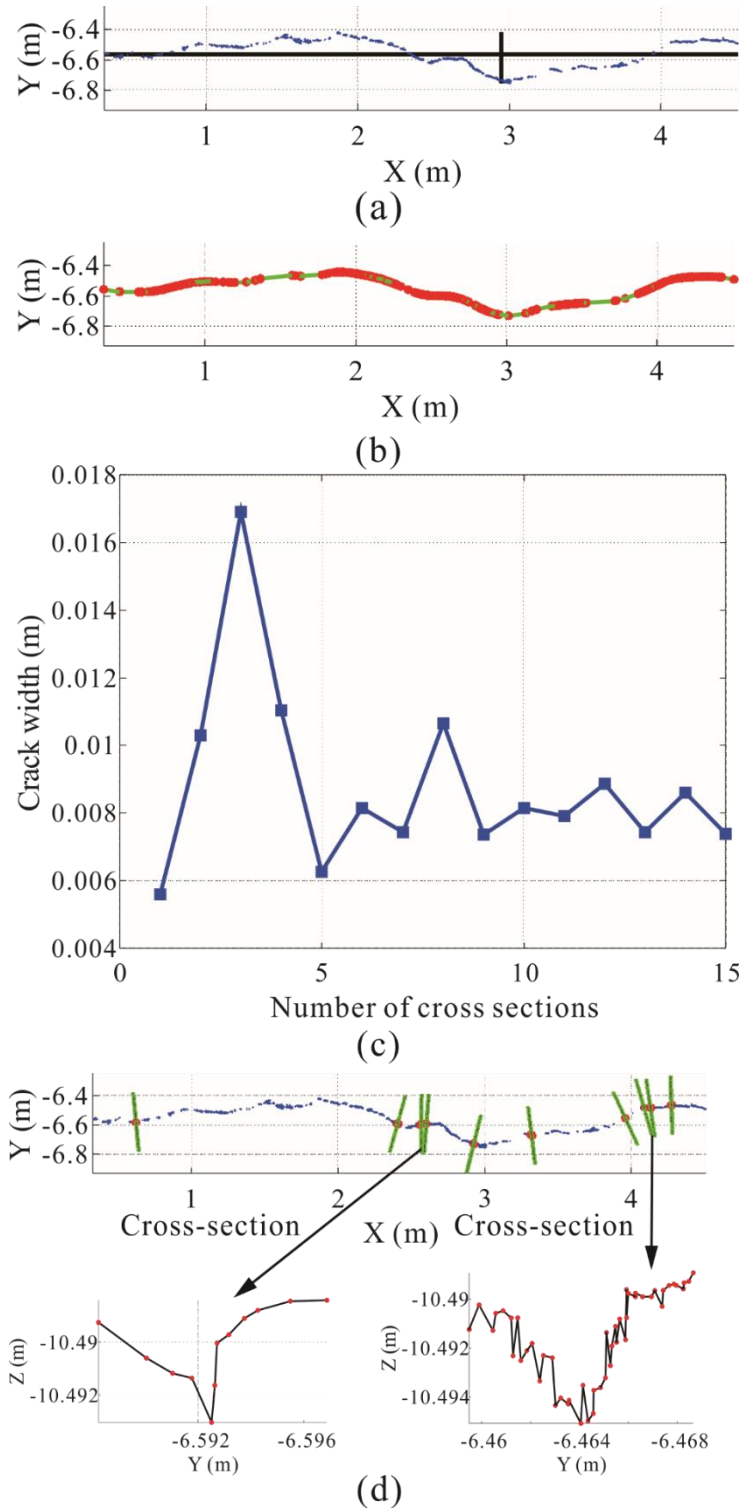


Figure 6 Crack characterization using projection and curve-skeleton methods : (a) the projection of crack on horizontal plane, (b) the skeleton of crack, (c) average width changes with the number of cross-section randomly selected from the crack point cloud, and (d) the locations of ten cross-sections.

3.5.3 Manual Crack Measurement

A cracking condition survey was also conducted to manually measure the length and width of the crack according to the Distress Identification Manual for the Long-Term Pavement Performance Program (Miller and Bellinger 2014), and its length and width are also included in Table 2.

The distance between the two ends of the crack was measured along X direction to represent the length of this crack using a projection algorithm. Thus, the projected length of this crack was less than those for the curve-skeleton algorithm and manual measurement, where the length of the curved crack was measured. Additionally, there are different definitions of the width and depth in the three methods. The maximum distances among the points along YZ directions were regarded as width and depth in the projection method, while the perpendicular distance between two lines of the crack was the width. Due to the curve-shape of the crack, the projected width and depth of this crack were larger than those obtained by the manual measurement and cross-section method. As can be seen from Table 2, the lengths obtained from the manual measurement and projection algorithm were close (4.18m, and 4.185m respectively), but smaller than those obtained from the curve-skeleton algorithm (4.285m). The results were reasonable since measurements obtained from the 3D reconstruction can obtain more accurate results with more detailed information regarding the cracking. In addition, similar results confirmed a good agreement between the new method and current commonly-used manual measurement method.

Chapter. 4 Case Study

To test the robustness of the proposed method under more complex situations, cracks on a stair with multiple planes were selected as a case study, and the same laser scanner was used to collect the point cloud of the stair, oriented approximately perpendicular to the three vertical surfaces (Figure 7). The scan parameters are summarized in Table 1. The shapes and dimensions of cracks varied from step to step: the crack on the lower step had the maximum average length and depth (0.369 m and 0.025 m, respectively), while the crack on the upper step had the maximum average width (0.015 m). The whole scanning lasted less than 10 minutes, and the resolution of the obtained point cloud was approximate 3 mm, which made it possible to capture more details as well as the points inside the cracks. After removing the undesired and noise data in pre-processing, there were 1,496,291 points remaining. A similar point density was observed in these stair planes, and optimal N selection did not consider the effect from the point density in this case. The front and side views of the stair are also shown in Figure 7, and it can be seen that the point distribution in crack areas is different from that in non-crack areas. Sparser points were observed in the crack area (front view). Because points inside of the crack were collected during laser scanning, more irregularity was found in the crack areas compared to non-crack areas (side view).

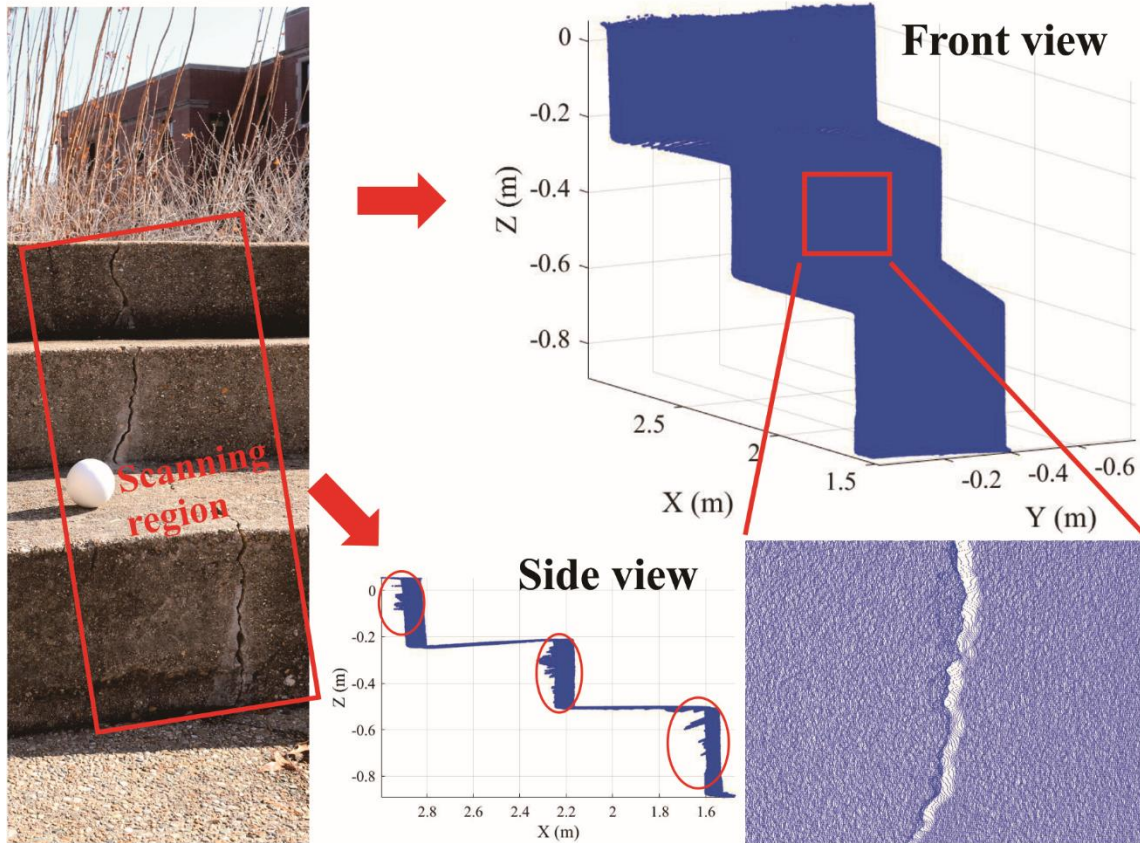


Figure 7 Point clouds collection of cracks in the stair case.

Figure 8 (a-n) shows the changes of point normal with a different number of nearest neighbor points in the stair case. When N was set less than 100, more differences on the point normal distribution were observed, even on the relatively smooth stair planes. When N was specified more than 500, the point normal distribution cannot accurately reflect the cracks' positions. Good results were obtained when choosing the N ranging from 100 points to 500 points, matching the N range ($100 \text{ points} \leq N \leq 539 \text{ points}$) calculated based on the average point density ($46.8768 \text{ points/cm}^3$) using Eq. 5. Furthermore, the exact computational time for point normal calculations with different N was measured using Tic & Toc functions in MATLAB software. Figure 8(o) illustrates the curve of elapsed time vs. N considered in the point normal calculation, and a linear relationship between them was observed. The computational time increased with the increase of the N . To save the computational time and improve computational efficiency, 100 neighbor points were eventually selected to calculate the point normal and point normal variance in this example.

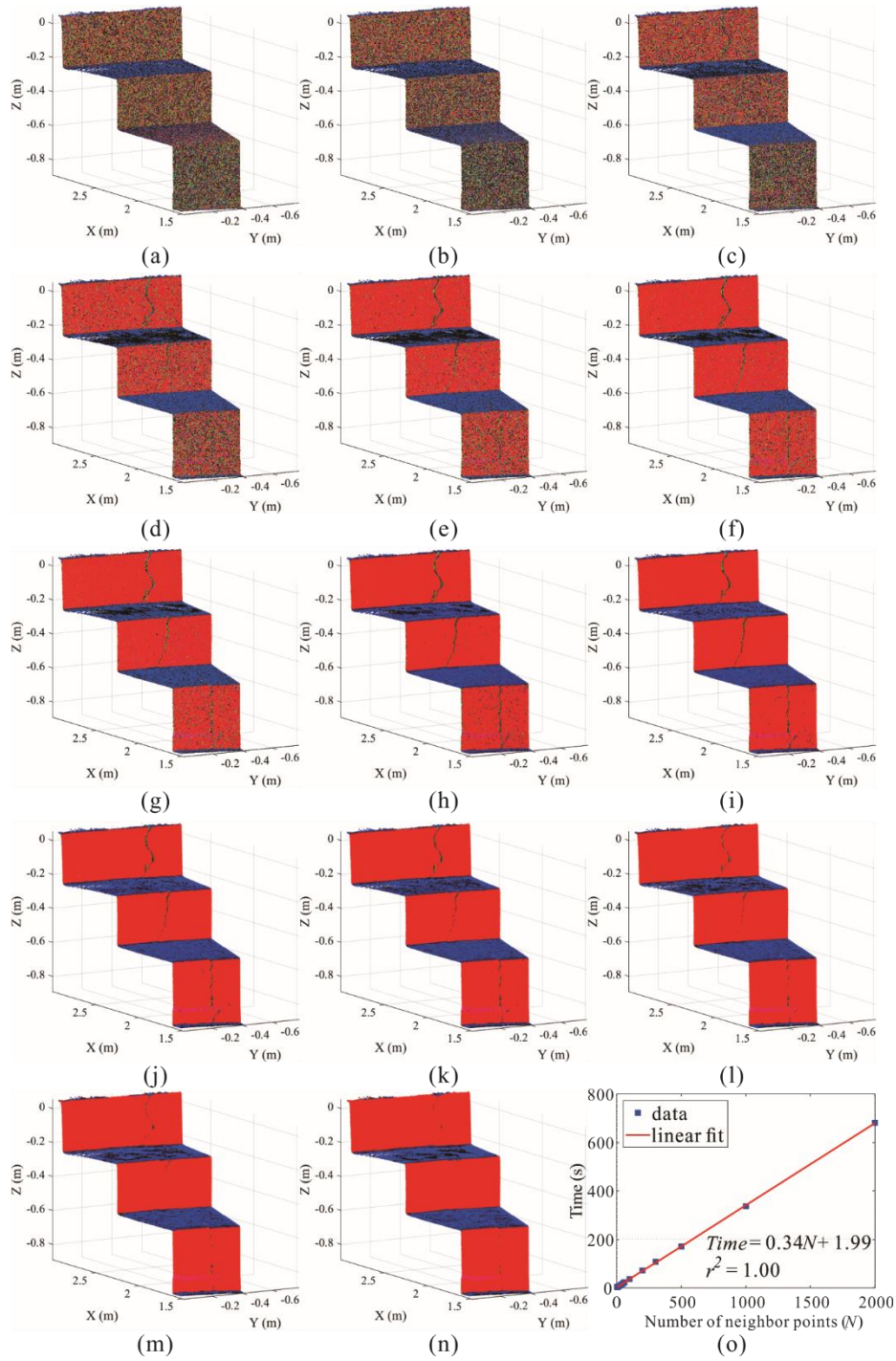


Figure 8 Variance of point normal vectors and computational time of point normal calculations with different neighboring points : (a) $N = 3$, (b) $N = 5$, (c) $N = 10$, (d) $N = 20$, (e) $N = 30$, (f) $N = 40$, (g) $N = 50$, (h) $N = 60$, (i) $N = 100$, (j) $N = 200$, (k) $N = 300$, (l) $N = 500$, (m) $N = 1000$, (n) $N = 2000$, and (o) plot of computational time vs. N .

Figure 9a shows the normal variance distribution of the stair point cloud based on Eq. 1 with

considering 100 nearest neighbor points. It is obvious that the cracks, stair edges, and dents had high normal variance compared to horizontal and vertical stair planes. They were identified from point clouds using the k-means clustering algorithm (Figure 9b). The horizontal stair edges and vertical cracks were detected in the upper stair region. Many dents on the lower two stair surfaces were also identified, besides the edges and cracks.

Note that the situation of the ground case is simpler than this stair case, because cracks only need to be identified from one single ground surface without the interference from multiple planes. It is also needed to remove the edges from the point clouds in the stair case in addition to the dents. The stair edges are located on the intersections of two adjacent stair planes and aligned horizontally; as a result, the points on the stair edges have similar z-coordinates. Consequently, they can be removed by specifying the lower and upper margins. Another k-means clustering was performed to classify all boundary points (cracks, dents, and stair edges) into three sets based on the stair location (x-coordinates), because there were three stairs in total in this case. The second clustering results are shown in Figure 9c, and detected points in the upper, middle, and lower stairs were marked blue, green, and red based on their x-coordinates, respectively. If the points' z-coordinates were less than the lower margin but larger than the upper margin, they were considered as the points located on the horizontal stair edges, and then removed after the second clustering. For example, in the case of the upper stair, the maximum and minimum z-coordinates of all points' z-coordinates were 0.053 m and -0.2486. The upper and lower margins were set as 0.015 m and 0.020 m, respectively, and the points with z-coordinates ranging from -0.2286 m to 0.038 m were retained as the point clouds of cracks and dents. It is suggested that the margins be selected based on the thickness of points on the stair edges. Figure 9d shows the point clouds of cracks and dents after removing the horizontal edges in the upper, middle, and lower stairs, respectively.

Figure 9e shows the real condition of the lower stair. Its surface was not a perfect plane with many dents on it, which was consistent with the analysis results. Due to the high resolution of TLS, these tiny damages on the concrete surfaces could be captured and were removed through the alpha-shape algorithm and volume threshold. Figure 9f shows the final results of crack detection from the point clouds.

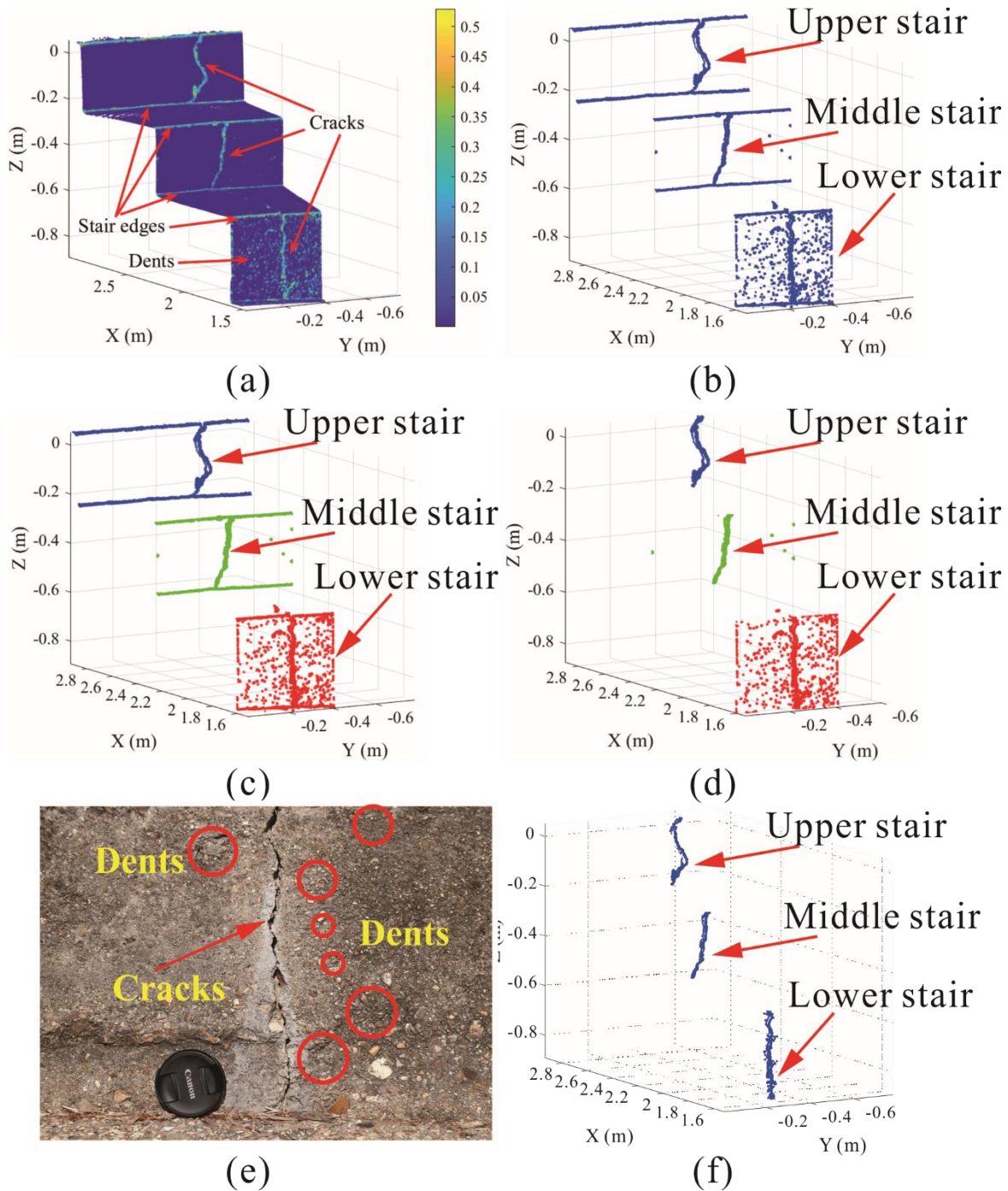


Figure 9 Cracks detection from point clouds in the stair case : (a) normal variance distribution, (b) cracks, stair edges, and dents extraction, (c) second clustering (different colors indicate different kinds of boundaries), (d) horizontal stair edges removal, (e) photo of the lower stair surface, and (f) small-scale dents removal.

Subsequently, the procedure of crack characterization was performed to determine the projected and real dimension of cracks in the stair. Figure 10 shows the projection results obtained using the PCA algorithm, and original point clouds of three cracks are in blue and projected are in red. In the projected

point clouds, the orthogonal black lines indicate the major, middle, and minor axes, respectively. Figure 11 shows the curve-skeletons of cracks in the stair which were found using the L_1 -median skeleton algorithm and used to measure the real length of cracks. The green lines are the curve-skeletons and red balls are the key points. Ten cross-sections perpendicular to the crack were selected at random for each crack to calculate the real width and depth of the cracks. Additionally, v-shaped cracks were observed on the cross-section (Figure 12). The results are summarized in Table 2. Similar to the ground case, the real dimensions matched the manual measurements, but with higher accuracy, indicating the good performance of the proposed methods.

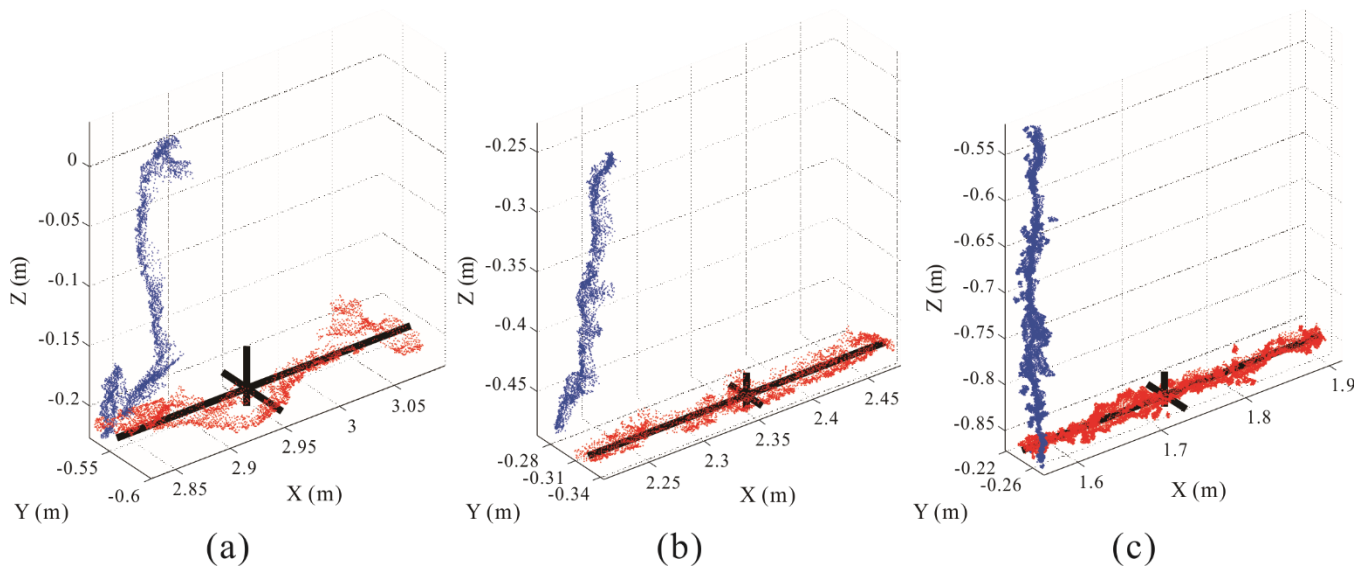


Figure 10 Projection of the crack point clouds : (a) upper stair, (b) middle stair, and (c) lower stair (original point clouds are marked as blue, point clouds after transformation are marked as red, and principal axes of point clouds are represented by black lines)

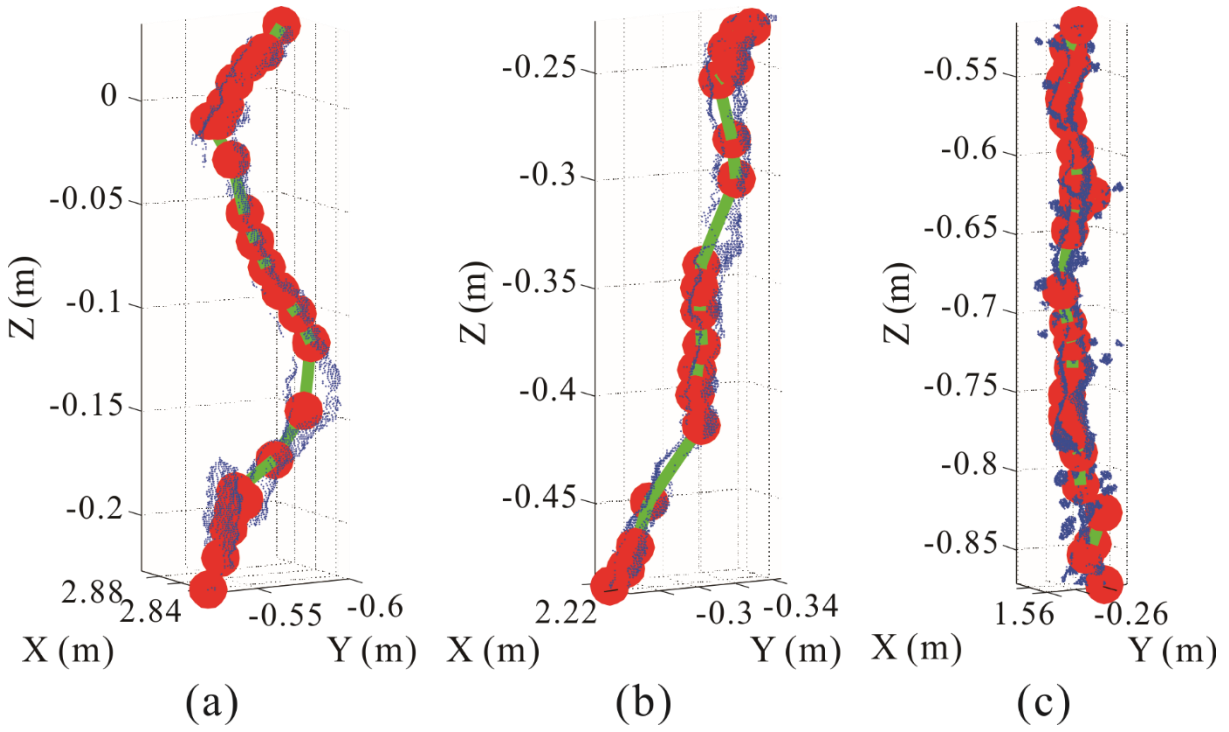


Figure 11 Curve-skeleton of the crack point clouds : (a) upper stair, (b) middle stair, and (c) lower stair (green lines are the curve skeletons, red balls are the key points in skeletons, and blue dots are the point clouds of cracks)

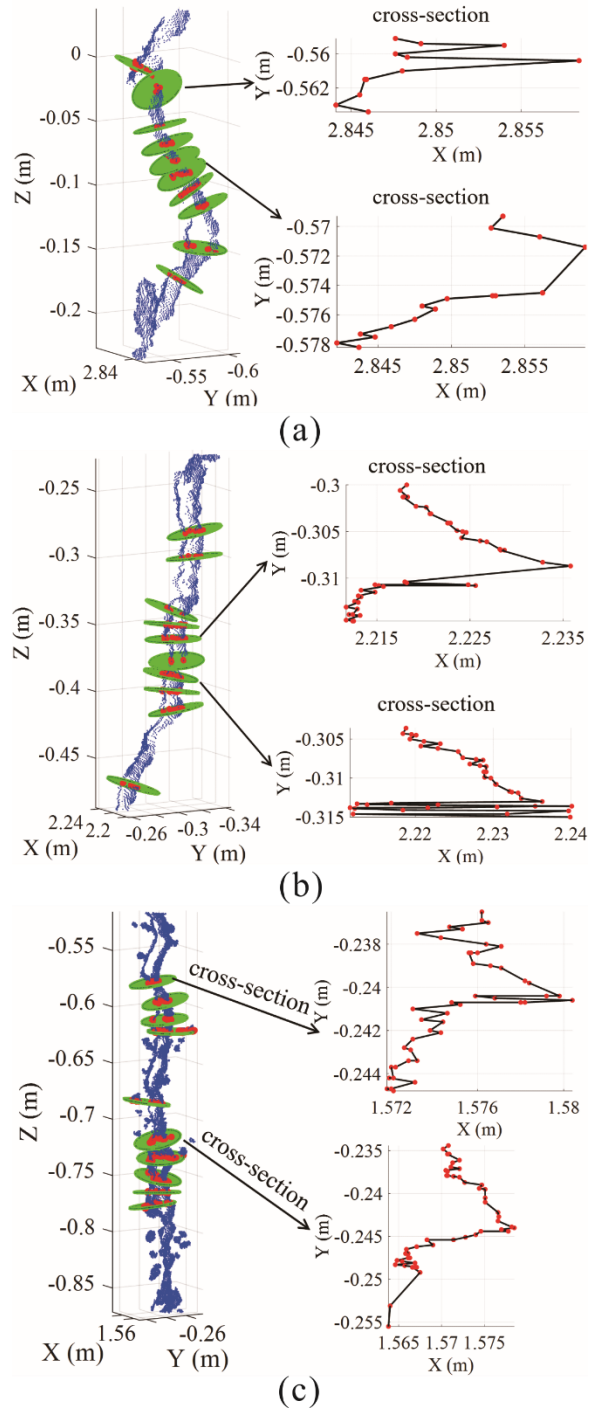


Figure 12 Ten cross-sections selected in the point clouds of cracks : (a) upper stair, (b) middle stair, and (c) lower stair (green circles are the cross-sections, and red dots are the points on the cross-sections)

The computational time for each procedure in two cases was recorded under the same computer configuration, using the Tic & Toc functions in MATLAB software. Table 3 shows the duration that the

developed method was taken for each step during the crack detection and characterization. The total computational time included three parts: (1) point normal calculation and crack and dents based on point normal variance; (2) small-scale dents removal, projection dimension of crack, and real dimension of crack (width and depth); (3) real dimension of crack (length). Eventually, 41.343 s was cost totally for the concrete ground case and 98.054 s for the concrete stair case, respectively, indicating the high efficiency and feasibility of the proposed method in this study.

Table 3 Computational time of crack detection and characterization for two cases.

Case / Item	Computational time (s)				Total time
	1. Point normal calculation	1. Small-scale dents removal	1. Real dimension of crack (length)	2. Cracks and dents extraction based on point normal variance	
Ground surface	16.661		24.682		41.343
Stair	85.305	7.388		5.361	98.054
Computer configuration	<ul style="list-style-type: none"> ● Laptop brand: Dell Precision 5530 BTX BASE ● Processor: Intel (R) Core (TM) i9-8950HK Six Core, CPU @ 2.90 GHz 2.90 GHz ● Installed memory (RAM): 16.00 GB (15.7 GB usable) ● Operating system: Windows 10 Home Edition (64-bit) 				

Chapter. 5 Summary and Conclusions

An approach was developed to automatically detect and characterize the cracks on concrete structures from the 3D point clouds in this study. The point normal variance was selected as the index to locate the cracks, and two methods (coordinate transformation and curve-skeletons & cross-sections) were used to determine the projected and real dimensions of cracks, respectively. In the crack detection process, kNN and PCA algorithms were used to determine the point normal, and k-means clustering and alpha-shape algorithms were employed to remove the undesired data concerning surfaces, horizontal stair edges, and small dents. In the crack characterization process, the coordinate transformation was performed to find the major, middle, and minor axis of cracks to calculate the projected dimensions. Furthermore, curve-skeletons and cross-sections of cracks were extracted to represent the real dimensions. The example and one case study demonstrated good agreements of results between the manual measurements and the real dimensions of cracks which were calculated using the developed method. In addition, the developed method can automatically capture more details of the cracking from 3D point clouds. It can be used to conduct complete processing and analysis for different conditions with accurate results. In a summary, the developed method enables a fast, accurate measurement and more comprehensive analysis for crack detection and characterization.

It was found that the point normal calculation highly depends on the number of neighbor points. The number of nearest neighbor points was suggested to be selected taking the point density into account. It's recommended that more case studies in various infrastructures such as bridges and buildings are needed to further validate the approach developed.

This method was developed to identify and characterize cracks only based on the point clouds. Therefore, the method can be suitable for any other measuring techniques which collect the high-resolution point clouds of the cracks, such as the portable laser scanning and photogrammetry. More case studies using other measuring techniques are needed to explore the wider application of this method. Additionally, for the small-scale cracks (e.g., less than a few millimeters in width), the terrestrial laser scanner is not able to collect the detailed morphological information inside of the cracks

due to its resolution limitations. In this case, the color information is highly recommended to be added to identify the cracks instead of the geometric data only.

References

- Au, O. K. C., Tai, C. L., Chu, H. K., Cohen-Or, D., and Lee, T. Y. (2008). "Skeleton extraction by mesh contraction." *ACM Transactions on Graphics*, 27(3), pp. 1-10.
- Avila, M., Begot, S., Duculty, F., and Nguyen, T. S. (2014). "2D image based road pavement crack detection by calculating minimal paths and dynamic programming." In *Proceedings of the 2014 IEEE International Conference on Image Processing (ICIP)*, pp. 783-787. Paris: IEEE.
- Bandis, S. C., Lumsden, A. C., and Barton, N. R. (1983). "Fundamentals of rock joint deformation." *International Journal of Rock Mechanics and Mining Sciences & Geomechanics Abstracts*, 20(6): pp. 249-268.
- Bose, P., Maheshwari, A., and Morin, P. (2003). "Fast approximations for sums of distances, clustering and the Fermat–Weber problem." *Computational Geometry*, 24(3), pp. 135-146.
- Cha, Y. J., Choi, W., and Büyüköztürk, O. (2017). "Deep learning-based crack damage detection using convolutional neural networks." *Computer-Aided Civil and Infrastructure Engineering*, 32(5), pp. 361-378.
- Cheung, Y. M. (2003). "k*-Means: A new generalized k-means clustering algorithm." *Pattern Recognition Letters*, 24(15), pp. 2883-2893.
- Cornea, N. D., Silver, D., and Min, P. (2007). "Curve-skeleton properties, applications, and algorithms." *IEEE Transactions on Visualization & Computer Graphics*, 13(3), pp. 530-548.
- Deng, Z., Zhu, X., Cheng, D., Zong, M., and Zhang, S. (2016). "Efficient kNN classification algorithm for big data." *Neurocomputing*, 195, pp. 143-148.
- Dung, C. V. (2019). "Autonomous concrete crack detection using deep fully convolutional neural network." *Automation in Construction*, 99, pp. 52-58.
- Edelsbrunner, H., Kirkpatrick, D.G., and Seidel, R. (1983). "On the shape of a set of points in the plane." *IEEE Transactions on information theory*, 29(4), pp. 551-559.
- Ester, M., Kriegel, H. P., Sander, J., and Xu, X. (1996, August). "A density-based algorithm for discovering clusters in large spatial databases with noise." In *Proceedings of the KDD*, pp. 226-231. Portland: AAAI.

- Falcão, A., Feng, C., Kustra, J., and Telea, A. (2017). "Multiscale 2D medial axes and 3D surface skeletons by the image foresting transform." In *Skeletonization: Theory, Methods and Applications*, 43-70. Cambridge: Academic Press.
- Fei, Y., Wang, K. C., Zhang, A., Chen, C., Li, J. Q., Liu, Y., and Li, B. (2019). "Pixel-Level Cracking Detection on 3D Asphalt Pavement Images Through Deep-Learning-Based CrackNet-V." *IEEE Transactions on Intelligent Transportation Systems*, 21(1), pp. 273-284.
- Ge, Y., Tang, H., Xia, D., Wang, L., Zhao, B., Teaway, J. W., and Zhou, T. (2018). "Automated measurements of discontinuity geometric properties from a 3D-point cloud based on a modified region growing algorithm." *Engineering Geology*, 242, pp. 44-54.
- Gui, R., Xu, X., Zhang, D., Lin, H., Pu, F., He, L., and Cao, M. (2018). "A component decomposition model for 3D laser scanning pavement data based on high-pass filtering and sparse analysis." *Sensors*, 18(7), 2294.
- Hamerly, G., & Elkan, C. (2004). "Learning the k in k-means." *Advances in neural information processing systems*, 16, pp. 281-288.
- Hoang, N. D., Nguyen, Q. L., and Tien Bui, D. (2018). "Image processing-based classification of asphalt pavement cracks using support vector machine optimized by artificial bee colony." *Journal of Computing in Civil Engineering*, 32(5), 04018037.
- Huang, H. W., Li, Q. T., and Zhang, D. M. (2018). "Deep learning based image recognition for crack and leakage defects of metro shield tunnel." *Tunnelling and Underground Space Technology*, 77, pp. 166-176.
- Huang, H., Wu, S., Cohen-Or, D., Gong, M., Zhang, H., Li, G., and Chen, B. (2013). "L1-medial skeleton of point cloud." *ACM Transactions on Graphics*, 32(4), pp. 65-1.
- Jahanshahi, M. R., Jazizadeh, F., Masri, S. F., and Becerik-Gerber, B. (2013). "Unsupervised approach for autonomous pavement-defect detection and quantification using an inexpensive depth sensor." *Journal of Computing in Civil Engineering*, 27(6), pp. 743-754.
- Jovančević, I., Pham, H. H., Orteu, J. J., Gilblas, R., Harvent, J., Maurice, X., and Brèthes, L. (2017). "3D point cloud analysis for detection and characterization of defects on airplane exterior surface." *Journal of Nondestructive Evaluation*, 36(4), 74.
- Kaseko, M. S., and Ritchie, S. G. (1993). "A neural network-based methodology for pavement crack detection and classification." *Transportation Research Part C: Emerging Technologies*, 1(4), pp. 275-291.

- Kim, M. K., Sohn, H., and Chang, C. C. (2014). "Localization and quantification of concrete spalling defects using terrestrial laser scanning." *Journal of Computing in Civil Engineering*, 29(6), 04014086.
- Kirschke, K. R., and S. A. Velinsky. (1992). "Histogram-based approach for automated pavement-crack sensing." *Journal of Transportation Engineering* 118(5), pp. 700-710.
- Klasing, K., Althoff, D., Wollherr, D., and Buss, M. (2009). "Comparison of surface normal estimation methods for range sensing applications." In *Processing of the 2009 IEEE International Conference on Robotics and Automation*, 3206-3211). Kobe: IEEE.
- Laefer, D. F., Truong-Hong, L., Carr, H., and Singh, M. (2014). "Crack detection limits in unit based masonry with terrestrial laser scanning." *Ndt & E International*, 62, pp. 66-76.
- Laflamme, S., Kollosche, M., Connor, J. J., and Kofod, G. (2012). "Soft capacitive sensor for structural health monitoring of large-scale systems." *Structural Control and Health Monitoring*, 19(1), pp. 70-81.
- Lee, B. J., and Lee, H. D. (2004). "Position-invariant neural network for digital pavement crack analysis." *Computer-Aided Civil and Infrastructure Engineering*, 19(2), pp. 105-118.
- Li, G., Zhao, X., Du, K., Ru, F., and Zhang, Y. (2017). "Recognition and evaluation of bridge cracks with modified active contour model and greedy search-based support vector machine." *Automation in Construction*, 78, pp. 51-61.
- Miller, J. S. and Bellinger, W. Y. (2014). "Distress identification manual for the long-term pavement performance program (Fifth revised edition)." FHWA-HRT-13-092, Office of Infrastructure Research and Development, Federal Highway Administration, McLean VA.
- Mohan, A., and Poobal, S. (2018). "Crack detection using image processing: A critical review and analysis." *Alexandria Engineering Journal*, 57(2), pp. 787-798.
- Nakaniwa, K., Yabuki, N., Nishi, D., Mitani, K., and Matsumoto, M. (2014). "Development and Applications of a Total Station with a Built-in Crack Scale." In *Processing of the 2014 International Conference on Computing in Civil and Building Engineering*, pp. 1755-1762. Orlando: ASCE.
- Napolitano, R., and Glisic, B. (2019). "Methodology for diagnosing crack patterns in masonry structures using photogrammetry and distinct element modeling." *Engineering Structures*, 181, pp. 519-528.
- Nguyen, T. S., Avila, M., and Begot, S. (2009). "Automatic detection and classification of defect on

- road pavement using anisotropy measure." In 2009 17th European Signal Processing Conference, pp. 617-621. Glasgow: IEEE.
- Nishiyama, S., Minakata, N., Kikuchi, T., and Yano, T. (2015). "Improved digital photogrammetry technique for crack monitoring." *Advanced Engineering Informatics*, 29(4), pp. 851-858.
- Oliveira, H., and Correia, P. L. (2009). "Automatic road crack segmentation using entropy and image dynamic thresholding." In *Processing of the 2009 17th European Signal Processing Conference*, pp. 622-626. Glasgow: IEEE.
- Olsen, M. J., Kuester, F., Chang, B. J., and Hutchinson, T. C. (2010). "Terrestrial laser scanning-based structural damage assessment." *Journal of Computing in Civil Engineering*, 24(3), pp. 264-272.
- Rabah, M., Elhatab, A., and Fayad, A. (2013). "Automatic concrete cracks detection and mapping of terrestrial laser scan data." *NRIAG Journal of Astronomy and Geophysics*, 2(2), pp. 250-255.
- Ritdumrongkul, S., and Fujino, Y. (2007). "Identification of the location and size of cracks in beams by a piezoceramic actuator–sensor." *The Journal of the International Association for Structural Control and Monitoring*, 14(6), pp. 931-943.
- Riquelme, A. J., Abellán, A., Tomás, R., and Jaboyedoff, M. (2014). "A new approach for semi-automatic rock mass joints recognition from 3D point clouds." *Computers & Geosciences*, 68, pp. 38-52.
- Santhi, B., G. Krishnamurthy, S. Siddharth, and P. K. Ramakrishnan. 2012. "Automatic detection of cracks in pavements using edge detection operator." *J. Theor. Appl. Inf. Technol.* 36 (2): 199–205.
- Sollazzo, G., Wang, K. C. P., Bosurgi, G., and Li, J. Q. (2016). "Hybrid procedure for automated detection of cracking with 3D pavement data." *Journal of Computing in Civil Engineering*, 30(6), 04016032.
- Valença, J., Dias-da-Costa, D., Júlio, E. N. B. S., Araújo, H., and Costa, H. (2013). "Automatic crack monitoring using photogrammetry and image processing." *Measurement*, 46(1), pp. 433-441.
- Valença, J., Puente, I., Júlio, E., González-Jorge, H., and Arias-Sánchez, P. (2017). "Assessment of cracks on concrete bridges using image processing supported by laser scanning survey." *Construction and Building Materials*, 146, pp. 668-678.
- Wang, K. C. (2004). "Challenges and feasibility for comprehensive automated survey of pavement conditions." In *Proceeding of the 8th International Conference on Applications of Advanced Technologies in Transportation Engineering (AATTE)*, 531-536. Beijing: ASCE.

- Zalama, E., Gómez-García-Bermejo, J., Medina, R., and Llamas, J. (2014). "Road crack detection using visual features extracted by Gabor filters." *Computer-Aided Civil and Infrastructure Engineering*, 29(5), pp. 342-358.
- Zhang, A., Wang, K. C., Fei, Y., Liu, Y., Chen, C., Yang, G., and Qiu, S. (2019). "Automated pixel-level pavement crack detection on 3D asphalt surfaces with a recurrent neural network." *Computer-Aided Civil and Infrastructure Engineering*, 34(3), pp. 213-229.
- Zhang, A., Wang, K. C., Li, B., Yang, E., Dai, X., Peng, Y., and Chen, C. (2017a). "Automated pixel-level pavement crack detection on 3D asphalt surfaces using a deep-learning network." *Computer-Aided Civil and Infrastructure Engineering*, 32(10), pp. 805-819.
- Zhang, A., Wang, K. C., and Ai, C. (2017b). "3D shadow modeling for detection of descended patterns on 3D pavement surface." *Journal of Computing in Civil Engineering*, 31(4), 04017019.
- Zhang, L., Yang, F., Zhang, Y. D., and Zhu, Y. J. (2016). "Road crack detection using deep convolutional neural network." In *Processing of the 2016 IEEE international conference on image processing (ICIP)*, 3708-3712. Phoenix: IEEE.
- Zhou, J., P. S. Huang, and F. P. Chiang. 2006. "Wavelet-based pavement distress detection and evaluation." *Opt. Eng.* 45 (2): 027007. <https://doi.org/10.1117/1.2172917>.
- Zou, Q., Cao, Y., Li, Q. Q., Mao, Q. Z., and Wang, S. (2012). "CrackTree: Automatic crack detection from pavement images." *Pattern Recognition Letters*, 33(3), pp. 227-238.